Journal of the Ceramic Society of Japan 119 [12] 909-915 2011 Paper

Inhomogeneous distribution of Na^+ in alkali silicate glasses

Yomei TOKUDA,† Takanori OKA, Masahide TAKAHASHI and Toshinobu YOKO

Institute for Chemical Research, Kyoto University, Uji, Kyoto 611–0011

We investigated the Na^+ environment in sodium silicate glasses and mixed alkali silicate glasses using ^{23}Na multiple-quantum magic-angle spinning (MQMAS) NMR spectroscopy, ab initio molecular orbital (MO) calculations, and Na^+ elution analysis. The ^{23}Na MQMAS NMR spectra of Na_2O–$xSiO_2$ and $(1-y)Na_2O$–yM_2O–$2SiO_2$ (M = Li, K) glasses showed an inhomogeneous distribution of local structures around Na^+, even though spectral deconvolution was impossible. The quantum chemical calculations indicated that the alkali silicate glasses contained both aggregated and isolated Na^+ sites. The elution behavior also supported the local structure distribution described above. These results indicated that a cation with a high cation field strength tends to aggregate in mixed silicate glasses.

Key-words : Sodium silicate, Mixed alkali, MQMAS NMR, Quantum chemical calculation, Na^+ elution behavior, Inhomogeneous distribution

[Received March 9, 2011; Accepted August 26, 2011]

1. Introduction

Alkali ions in an amorphous state have attracted much interest because of the mixed alkali effect (MAE), which corresponds to a deviation from the linear additivity property of glass in alkali oxide glasses when one type of alkali ion is replaced by another type.[1),2)] In fact, it is well known that the electric conductivity of alkali silicate glasses decreases when one type of alkali ion is replaced by another type. In general, a minimum electric conductivity is observed at some intermediate composition.

Various structural models have been proposed to explain the MAE based on a homogeneous spatial cation distribution using nuclear magnetic resonance (NMR) spectroscopy,[3),4)] extended X-ray absorption fine structure (EXAFS)[5),6)] analysis, and molecular dynamics (MD) simulation.[7)] Ingram et al.[1),5),6)] reported that the MAE is caused by the disturbance created when one type of alkali ion moves to sites previously occupied by another type of alkali ion. The transportation of alkali ions in a glass network is hindered when the network contains a different type of alkali ion; this hindrance is caused by site mismatch energy. Ab initio molecular orbital calculations[8),9)] and an XPS study support this assumption.[10)] More recently, an MD simulation using mixed alkali (Li–K) silicate glasses provided an inhomogeneous structural model, where the environment of each alkali ion was different from those of the other alkali ions.[11)] This study attributed the MAE to the site mismatch energy and a decrease in the hopping frequency of alkali ions between neighboring sites. Far-infrared spectroscopy on xCs_2O–$(1-x)Na_2O$–$5SiO_2$ glasses also showed that the vibrational energy generated by each cation is the same as that in the case of single alkali silicates.[12)] In addition, the ^{29}Si MAS NMR spectra of various types of single alkali silicates showed that the distribution of SiO_4 units, Q^n, which designates the tetrahedrally coordinated Si with n bridging oxygens and $(4-n)$ nonbridging oxygens, is determined by a species of alkali as $Q^n \leftrightarrow Q^{n+1} + Q^{n-1}$.[13)] This reaction proceeds to the right when the field strength (Z/r) increases. In fact, Stebbins indicated that when an ion with high field strength is substituted for one with low field strength (e.g., Li for Na), there is an increase in the mean number of nonbridging oxygens associated with the ion with high field strength.[14)]

Undoubtedly, additional work is required to characterize the local structure of the alkali ions in mixed alkali silicate glasses. Magic-angle spinning (MAS) NMR is one of the most powerful tools for investigating the local structure of ions in glasses, as shown above. However, the MAS NMR spectra of quadrupolar nuclei such as Na in an amorphous state often show a featureless line because a quadrupolar interaction significantly broadens the NMR line width. Dynamic angle spinning (DAS) NMR,[15),16)] double rotation (DOR) NMR,[17)] and MQMAS (multiple-quantum magic-angle spinning) NMR have been proposed by several authors[18)] to obtain the sharp spectra of quadrupolar nuclei. In particular, MQMAS NMR is a relatively simple method that can be applied to a classical MAS NMR spectrometer because it combines the MAS NMR apparatus and a pulse sequence.[18)] MQMAS NMR provides narrow two-dimensional spectra composed of a MAS dimension and an isotropic dimension. Although this method provides a considerable amount of information about the isotropic chemical shift and the quadrupolar interaction constants, especially in relation to network-forming ions such as ^{11}B, ^{17}O, and ^{27}Al, it is difficult to interpret the MQMAS spectra of alkali ions[19)–22)] because there is no well-defined alkali site in an amorphous solid.

The objective of this study is to interpret the featureless ^{23}Na MQMAS NMR spectra of silicate glasses and investigate the alkali ion distribution in these glasses using ab initio MO calculations, which have been widely utilized to simulate the structure of glass and calculate the NMR parameters.[23)–25)] Large cluster model calculations were employed to reproduce the local structure around the Na^+ in silicate glasses.

In this study, we applied ^{23}Na MQMAS NMR spectroscopy to Na_2O–SiO_2, Na_2O–K_2O–$2SiO_2$, and Na_2O–Li_2O–$2SiO_2$ glasses. We also simulated the local structure around the Na^+ in the silicate glasses and calculated the NMR parameters in order to assign the ^{23}Na MQMAS NMR spectra. We also confirmed

† Corresponding author: Y. Tokuda; E-mail: tokuda@noncry.kuicr.kyoto-u.ac.jp

whether this assignment was correct by carrying out a Na^+ elution analysis using distilled water.

2. Experimental procedure

2.1 Sample preparation

The following glass compositions were used in the MQMAS experiment: Na_2O–$xSiO_2$ ($x = 2$, 3), $(1-y)Na_2O$–yK_2O–$2SiO_2$, and $(1-y)Na_2O$–yLi_2O–$2SiO_2$ ($y = 0$, 0.25, 0.33, 0.5). The starting materials were Na_2CO_3, K_2CO_3, Li_2CO_3, and SiO_2 commercial powders. Glass batches with the prescribed compositions were melted in a Pt crucible at 1300–1400°C for 5 h. The melts were quenched by immersing the bottom of the Pt crucible in water, which resulted in the formation of an optically clear and colorless material. To reduce the spin relaxation times, 0.1 mol % Mn was added to the mixed alkali glasses because the long relaxation times were observed in such glasses. The silicate crystals, Na_2O–SiO_2 and α-Na_2O–$2SiO_2$ with no spin-relaxation additive, were also prepared by crystallizing glasses of the stoichiometric compositions.[26] The crystallinity was confirmed using X ray diffraction (RIGAKU, RINT 2100). The Na_2O–$3SiO_2$ composition was selected for the Na^+ elution analysis because the chemical durability of a high silica composition was too high, while that of a low silica composition was too low. The glass was crushed and size-classified using a steel mesh (106–212 µm). The crushed glass was washed five times using ethanol in order to eliminate any fine powder on the glass surfaces; the samples were then dried at 100°C.

2.2 NMR spectroscopy

Solid state ^{23}Na NMR spectra were acquired using a Chemagnetics CMX400 spectrometer. A commercial probe (4 mm) was used, and the rotation speed was set to 13 kHz with an accuracy of ±10 Hz. To obtain pure absorption spectra, a Z-filtering method[27] and hypercomplex phase cycling[28] were used. The first radio frequency (rf) pulse in the MQMAS NMR experiment was set to 6.8 µs, while the second rf pulse was set to 2.2 µs. The spectra were obtained with a cycle time of 2 s. In the case of the silicate crystal, the cycle time was set to 60 s. The NMR signals were processed using Fourier transformation with shearing transformation. The MAS and isotropic dimensions were reported in ppm relative to NaCl (aq), whose MAS and isotropic shifts are set to 0 ppm.

2.3 MO calculation

We used three types of clusters for modeling the local structure around the Na in the silicate glasses (**Fig. 1**). A cluster with one Na atom was designated as silicate_Q3, where Q^n represents Si with n bridging oxygens and $(4-n)$ nonbridging oxygens. We used two types of clusters with three Na atoms. One cluster was designated as silicate_Q3Q3Q3, which had three Q3 sites, and the other cluster was designated as silicate_Q2Q3, which had one Q3 site and one Q2 site. Silicate_Q3Q3Q3 simulated aggregated Na^+, while silicate_Q3 simulated isolated Na^+. All of these clusters had eight Si atoms and exhibited a ring structure. The Na atoms were adjacent to both the bridging and nonbridging oxygens. These clusters were terminated by H atoms to compensate for the charge of the clusters. The clusters were completely optimized at the Hartree–Fock (HF) level with 6-31G(d) basis sets. The ^{23}Na NMR shielding constants and Mulliken charges were also obtained at the HF/6-31G(d) level using the gauge-independent atomic orbital (GIAO) method. The electric field gradients were calculated to obtain the asymmetry parameters and the quadrupolar shifts.

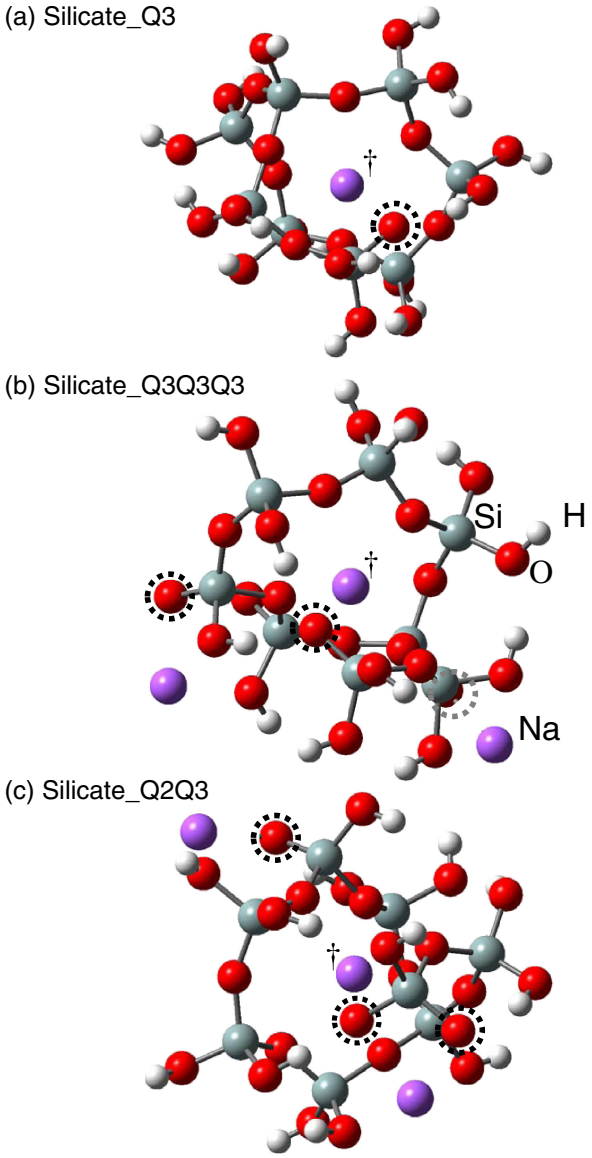

Fig. 1. (Color online) Optimized structures of (a) silicate_Q3, (b) silicate_Q3Q3Q3, and (c) silicate_Q2Q3. Geometry optimization was performed at HF/6-31G(d). Chemical shifts of ^{23}Na with daggers were calculated to be 566.2, 566.6, and 563.5 ppm for silicate_Q3, silicate_Q3Q3Q3, and silicate_Q2Q3, respectively. Dotted lines indicate the non-bridging oxygens.

All the ab initio MO calculations were performed using Gaussian 03[29] on an SGI Origin 3800 at the Supercomputer Laboratory, Institute for Chemical Research, Kyoto University.

2.4 Na^+ elution analysis

The crushed glass samples (300 mg) were soaked in 50 ml of distilled water at 40°C. The Na^+ concentration in the water was monitored using a sodium ion meter, CARDY C-122 (HORIBA). The MQMAS NMR spectra were also acquired for these sodium-eluted glasses.

3. Results

The ^{23}Na MQMAS NMR spectra of $(1-y)Na_2O$–yK_2O–$2SiO_2$ ($y = 0$, 0.25, 0.33, 0.5) glasses are shown in **Figs. 2**(a)–2(d). The horizontal and vertical axes are the MAS and isotropic dimensions, respectively. The MQMAS NMR spectra of the $(1-y)Na_2O$–xLi_2O–$2SiO_2$ ($y = 0.25$, 0.5) glasses are shown in

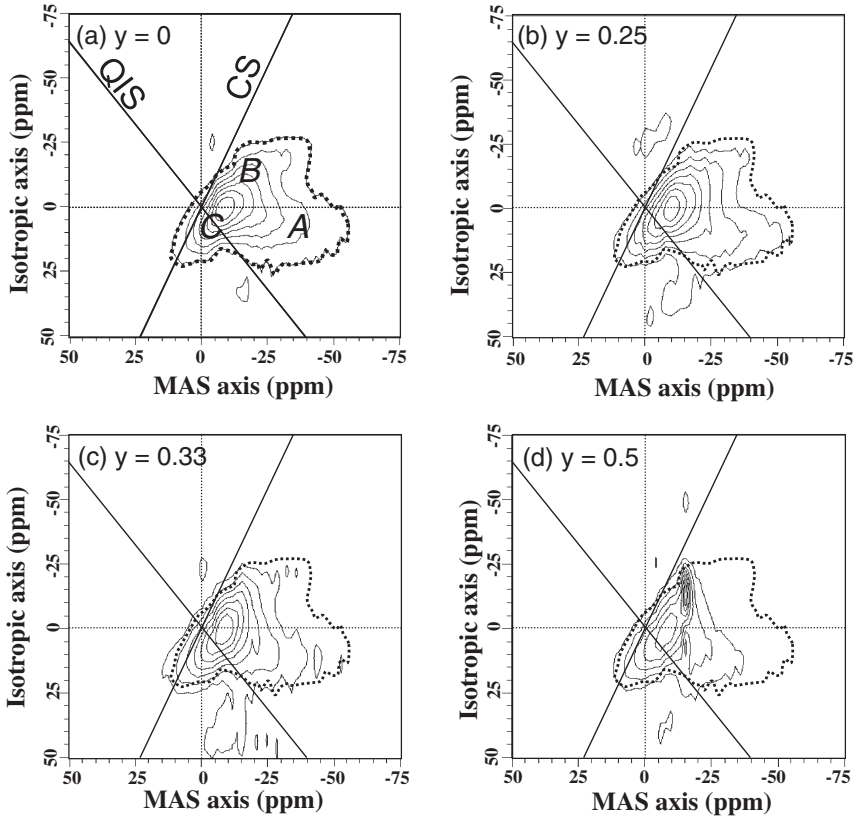

Fig. 2. ^{23}Na MQMAS NMR spectra of $(1-y)Na_2O$–yK_2O–$2SiO_2$ glass ($y = 0$, 0.25, 0.33, 0.5). The dotted lines in the figures correspond to the 12.5% height lines of the ^{23}Na MQMAS NMR spectrum of Na_2O–$2SiO_2$ glass. The inset lines are the chemical shift (CS) axis and the quadrupolar interaction shift (QIS) axis. The notations A, B, and C show the isolated Na^+ to Q^3 Si, Na^+ adjacent to Q^2 Si, aggregated Na^+ adjacent to Q^3 Si, and, respectively.

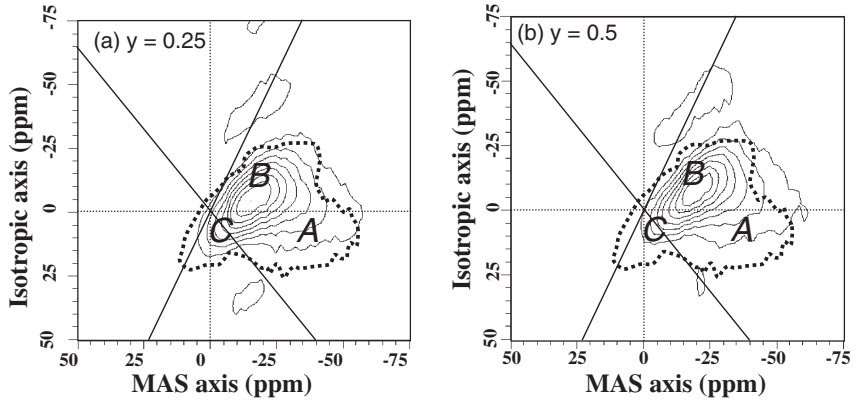

Fig. 3. ^{23}Na MQMAS NMR spectra of $(1-y)Na_2O$–yLi_2O–$2SiO_2$ glass ($y = 0.25$, 0.5). The dotted lines in the figures correspond to the 12.5% height lines of the ^{23}Na MQMAS NMR spectrum of Na_2O–$2SiO_2$ glass shown in Fig. 1(a). The inset lines are the chemical shift (CS) axis and the quadrupolar interaction shift (QIS) axis. The notations A, B, and C show the Na^+ adjacent to Q^2 Si, aggregated Na^+ adjacent to Q^3 Si, and isolated Na^+ to Q3 Si, respectively.

Figs. 3(a) and 3(b). The contour lines are plotted at every 12.5%, while the dotted line and circle at the center of the spectra correspond to 12.5 and 87.5%, respectively. The two intersecting solid lines shown in Figs. 2 and 3 indicate a chemical shift (CS) axis and a quadrupolar interaction shift (QIS) axis, respectively. The dotted lines in these figures correspond to the 12.5% height line of the ^{23}Na MQMAS NMR spectrum of Na_2O–$2SiO_2$ glass, shown in Fig. 2(a). It is obvious that the area around −40 ppm on the MAS axis disappears when Na_2O is replaced with K_2O, as shown in Fig. 2, while the area around 0 ppm disappears when Na_2O is replaced with Li_2O, as shown in Fig. 3. Spectral deconvolution was impossible because there was no distinct peak in the spectra.

The MQMAS NMR spectra of the silicate crystals were also shown in **Fig. 4**. The peak position of α-Na_2O–$2SiO_2$ crystal is more negative in both MAS and isotropic axis than that of Na2O–SiO2 crystal.

In the Na^+ elution analysis, the mass of Na^+ in the water was calculated from the Na^+ concentration, as shown in **Fig. 5**. It was found that this mass was linearly dependant on the square root of the time within 48 h. **Figure 6** shows the MQMAS NMR spectra of the glasses before and after the elution analysis. These spectra

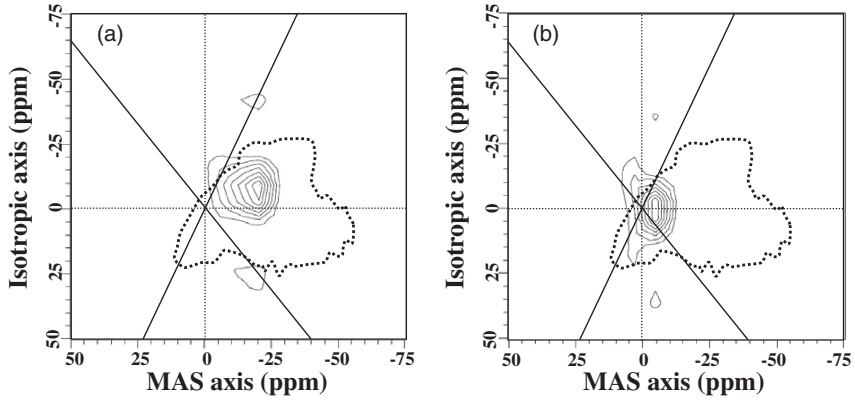

Fig. 4. ^{23}Na MQMAS NMR spectra of (a) Na_2O–$2SiO_2$ and (b) Na_2O–SiO_2 crystal. The dotted lines in the figures correspond to the 12.5% height lines of the ^{23}Na MQMAS NMR spectrum of Na_2O–$2SiO_2$ glass. The inset lines are the chemical shift (CS) axis and the quadrupolar interaction shift (QIS) axis.

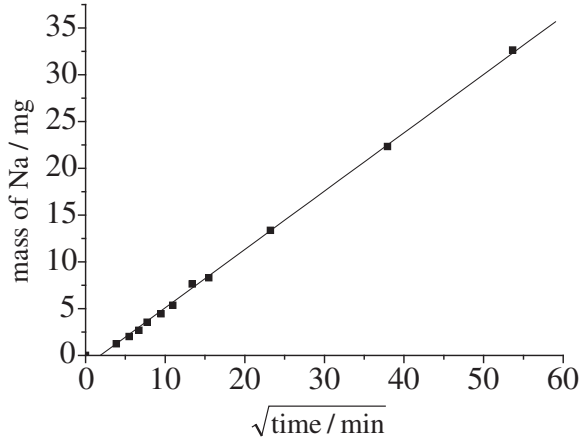

Fig. 5. Na mass plotted against the square root of the elution time. The time dependence is linear in this range.

are normalized because the volumes are proportional to the residual Na^+. The contour lines are plotted at every 12.5%. The isotropic chemical shift and quadrupolar interaction coupling constant were calculated as follows:[28]

$$\omega_{MAS} = \Delta\sigma + \Delta\sigma^{(2)}{}_{iso} \quad (1)$$

$$\omega_{iso} = 17/8 \times \Delta\sigma - 5/4 \times \Delta\sigma^{(2)}{}_{iso}, \quad (2)$$

where ω_{MAS}, ω_{iso}, $\Delta\sigma$, and $\Delta\sigma^{(2)}{}_{iso}$ are the MAS dimension, isotropic dimension, chemical shift, and quadrupolar shift, respectively. These parameters are listed in **Table 1**. The isotropic chemical shift shows an upfield shift after elution.

The ab initio MO calculations provided the optimized geometries of the model clusters, as shown in Fig. 1. The coordination number, C_N, for the central Na was defined as the number of the oxygens of which Na–O distances are bellow 2.6 Å. The enumerated C_Ns were 5 in the present model clusters. This result agrees with the previously reported experimental result.[30]

The calculated chemical shieldings of the central Na atoms in silicate_Q3, silicate_Q3Q3Q3, and silicate_Q2Q3 are 566.2, 566.6, and 563.5 ppm, respectively. The Mulliken charges of the oxygens are shown in **Table 2**. O_{nbr} represents the nonbridging oxygens adjacent to the central Na atoms. The average charges of the oxygens closest to the Na and the other oxygens are designated as $O_{nearest}$ and O_{others}, respectively. The $O_{nearest}$ and O_{others} charges of silicate_Q3Q3Q3 were greater than and equal to those of silicate_Q3, respectively. The $O_{nearest}$ charge of silicate_Q2Q3 was greater than the $O_{nearest}$ charges of silicate_Q3 and silicate_Q3Q3Q3, while the O_{others} charge of silicate_Q2Q3 was smaller than the O_{others} charges of silicate_Q3 and silicate_Q3Q3Q3.

Next, we obtained the electric field gradient, $V_{\alpha\alpha}$, from which the quadrupolar interaction can be calculated, as given below:

$$\eta = (V_{xx} - V_{yy})/V_{zz} \quad (3)$$

$$\nu_Q{}^2 \propto V_{zz}{}^2(1 + \eta^2/3), \quad (4)$$

where the parameters η and $\nu_Q{}^2$ refer to the asymmetry parameter and quadrupolar shift, respectively. The values of $V_{zz}{}^2(1 + \eta^2/3)$ were 0.0028, 0.0004, and 0.020 for silicate_Q3, silicate_Q3Q3Q3, and silicate_Q2Q3, respectively. **Table 3** lists these values calculated for the central Na in the clusters.

4. Discussion

4.1 Assignment of MQMAS NMR spectra

Firstly, the assignment based on the MQMAS NMR spectra of the silicate crystals is presented because the NMR shifts of the crystals show the similar manner to those of glasses. Previously it is reported that Na_2O–$2SiO_2$ and Na_2O–SiO_2 crystals have Q^3 and Q^2 site, respectively.[31),32)] As shown in Fig. 4, Na_2O–$2SiO_2$ crystal shows more negative shift in both MAS and isotropic axis than Na_2O–SiO_2 crystal does. This fact indicates that both the MAS and isotropic shift of Na adjacent to Q^2 site is more negative than that adjacent to Q^3 site. Based on this results, the peaks around B and C in Fig. 2 can be assigned to Q^3 and Q^2 site, respectively.

Second, the assignments based on the quantum chemical calculations are presented. We describe the relationship between the change in the NMR parameters and the shift in the MQMAS NMR spectrum. With an increase in the chemical shielding, the chemical shift decreases, which result in the upper right shift parallel to the CS axis according to Eqs. (1) and (2). On the other hand, the increase of the quadrapolar shift causes the lower right shift parallel to the QIS axis.

As previously reported, the ^{23}Na chemical shift increased with the Na^+ content.[14)] The ^{23}Na chemical shift was mainly affected by the nonbridging oxygens around the Na^+. This chemical shift trend was applicable to the distribution of the Na^+ in Na_2O–$2SiO_2$ glass. In fact, the local structure around Na in silicate_Q2Q3 and silicate_Q3 are similar to Na_2O–SiO_2 and Na_2O–$2SiO_2$ crystals, respectively. The calculated ^{23}Na chemical shift for silicate_Q2Q3 was smaller than the chemical shifts for silicate_Q3 and silicate_Q3Q3Q3, which result in lower left shift parallel to the CS axis. Accordingly, the lowest field area, that is, C in Fig. 2(a), corresponds to the Na^+ adjacent to silicon with a

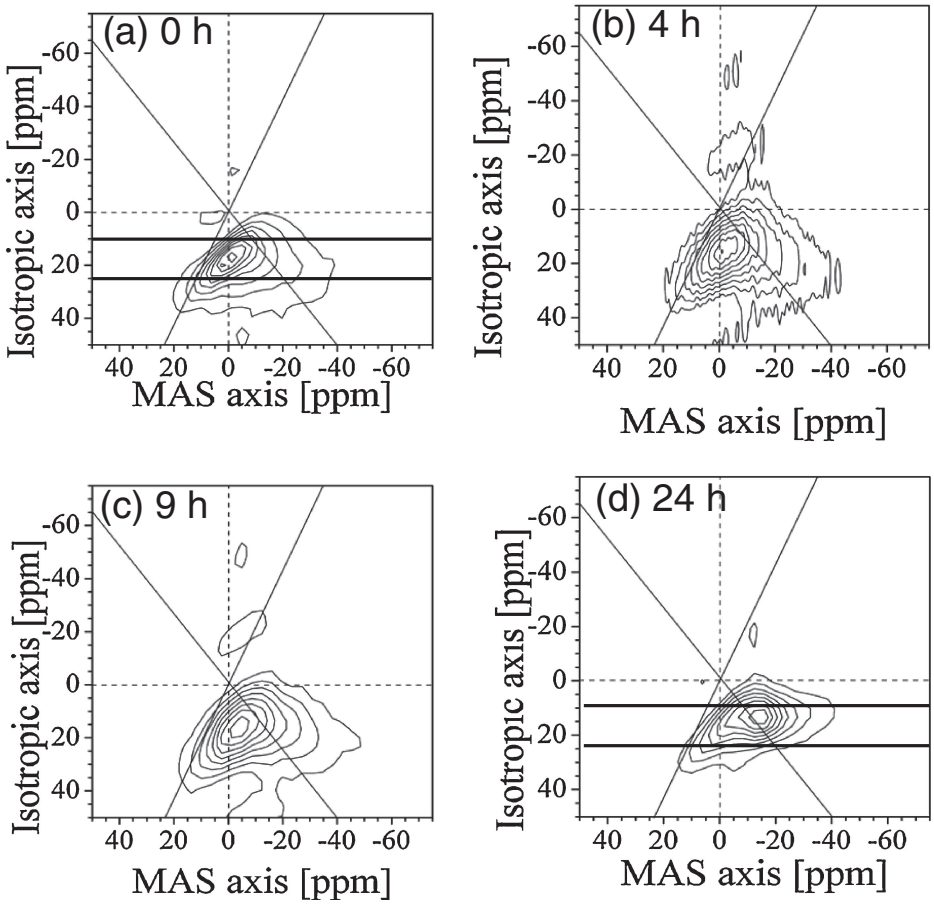

Fig. 6. MQMAS NMR spectra of Na_2O–$3SiO_2$ glass (a) before being immersed in distilled water and after being immersed for (b) 4 h, (c) 9 h, and (d) 24 h. Bold lines in (a) and (d) represent the cross sections shown in Fig. 6.

Table 1. Isotropic chemical shift $\Delta\sigma$ and the quadrupolar interaction coupling constant, $\Delta\sigma^{(2)}_{iso}$, for the samples eluted for 0 (as-prepared), 4, 9, and 24 h

Elution time/h	0	4	9	24
$\Delta\sigma$ (ppm)	4.9	3.2	3.3	−1.6
$\Delta\sigma^{(2)}_{iso}$ (ppm)	−5.6	−6.1	−7.3	−13.4

Table 2. Mulliken charges of the oxygens in the model clusters. O_{nbr} represents the nonbridging oxygens adjacent to the central Na's. Average charges of the oxygens nearest to Na, and other oxygens are designated as $O_{nearest}$ and O_{others}, respectively

Model	Oxygen		
	O_{nbr}	$O_{nearest}$	O_{others}
Q3	−0.99	−0.90	−0.86
Q3Q3Q3	−0.98	−0.92	−0.92
Q2	−1.07	−0.97	−0.76

Table 3. Calculated values of $V_{\alpha\alpha}$ for silicate_Q3 and silicate_Q3Q3Q3 (α = x, y, z). The asymmetry parameters were calculated using the equation $(V_{xx} - V_{yy})/V_{zz}$. The quadrupolar interaction shift is proportional to $V_{zz}(1 + 2/3)$. The calculated chemical shifts, σ, are also shown

Modeol	V_{xx}	V_{yy}	V_{zz}	η	$V_{zz}^2(1+\eta^2/3)$	σ (ppm)
Q3	0.020	0.030	−0.050	0.2	0.0028	566.2
Q3Q3Q3	0.0094	0.010	−0.019	0.03	0.0004	566.6
Q2Q3	−0.099	−0.030	0.13	0.53	0.020	563.5

large number of nonbridging oxygens at the Q^2 site. The present assignment agrees with that described above.

In the case of V_{zz} $(1 + \eta^2/3)$, the MO calculations failed to support the experimental results, because the value for silicate_Q2Q3 was larger than the values for silicate_Q3 and silicate_Q3Q3Q3, even though the predicted quadrupolar interaction shift of Na^+ related to the Q^2 site was less than that related to the Q^3 site. This is because the model cluster was so small that the oxygen charges and electric field gradient were not correctly produced. However, the lowest field area, that is, C in Fig. 2(a), was assigned to Q^2-related Na^+ because the iconicity of the system provided a symmetric field around the Na.

As shown in Table 2, silicate_Q3Q3Q3 is more ionic than silicate_Q3 because the $O_{nearest}$ and O_{others} charges are higher in silicate_Q3Q3Q3 than in silicate_Q3. Moreover, the charge distribution in silicate_Q3Q3Q3 is more symmetric than that in silicate_Q3 because the oxygen charges are equal in silicate_Q3Q3Q3, while they are not equal in silicate_Q3. As previously reported, symmetric charges around Na provide a small quadrupolar coupling constant.[33] In fact, the quadrupolar shift of silicate_Q3Q3Q3 is smaller than that of silicate_Q3. On the other hand, no difference between the chemical shifts of ^{23}Na was observed in a comparison between silicate_Q3 and silicate_Q3Q3Q3. Accordingly, the peak position of silicate Q3Q3Q3 should be more upper left parallel to the QIS axis than that of silicate Q3. On the other word, these results qualitatively indicated that the chemical shift of ^{23}Na near by a greater number of Na^+ provides upper left shift in Fig. 2. That is to say, the aggregated Na^+ corresponds to site B, shown in Fig. 2(a), while

the isolated Na^+ corresponds to site A, even though both Na^+ groups are adjacent to Q^3 silicon.

As Maekawa et al. indicated, the fractions of Q^2, Q^3, and Q^4 in the Na_2O–$2SiO_2$ glass were 10, 80, and 10%, respectively, using ^{29}Si MAS NMR.[13] The present ^{23}Na MQMAS NMR spectra were composed of sodiums around Q^2 and Q^3 Si. The volume of the spectra related to the Na^+ adjacent to Q^2 was smaller than that of the spectra related to the Na^+ adjacent to Q^3, even though the MQMAS NMR spectra lacked quantitativity because the triple quantum efficiency depended on the quadrupolar coupling constant. The exact area was not calculated because of the absence of a distinct peak in the spectra; however, the present assignment agrees qualitatively with the ^{29}Si MAS NMR results. This assignment also assumes that there was an inhomogeneous distribution of Na^+ in the sodium silicate glass.

Previously, using far infrared spectroscopy, Kamitos et al. indicated that several glasses with alkalis have an inhomogeneous distribution of alkali ions. They also suggested the formation of alkali-rich and -poor domains.[34),35)] In the notation of the present paper, these correspond to the aggregated and isolated sites, respectively. The present results are also in good agreement with the previous results.

4.2 Elution analysis

In order to clarify the present assumption, we next focus on the Na^+ elution analysis. In the case of Na_2O–$2SiO_2$ glass, it was difficult to control Na^+ leaching because Na_2O–$2SiO_2$ glass contained a large amount of Na_2O, which resulted in low durability. There was also an inhomogeneous distribution of Na^+ in Na_2O–$3SiO_2$ glass, as shown in Fig. 6(a). Therefore, Na_2O–$3SiO_2$ glass was selected instead of Na_2O–$2SiO_2$ glass, as mentioned in the experimental section. In the case of such an inhomogeneous distribution in glass, different elution rates were predicted for the isolated and aggregated sites.

First, we focus on the Na^+ concentration-time dependence. It is well known that in the case of linear dependence on the square root of time, the elution mechanism is the preferential extraction of alkali, while in the case of linear dependence on time, elution is caused by the breaking of siloxane bonds.[36)] In the present experiment, as shown in Fig. 5, the mass of the extracted Na^+ was linearly dependant on the square root of time, indicating that the elution of the Na^+ into the water was caused by ion exchange in Na_2O–$3SiO_2$ glass within 24 h. Therefore, the change in the spectra reflects the elutability of Na^+ at a specific site.

As shown in Fig. 6, the distribution of the Na^+ clearly changed during elution. Here, the spectra are normalized because their area is proportional to the Na^+ content. Therefore, it is possible to compare the elution rate of a particular Na^+ site with that of the other Na^+ sites, even though MQMAS NMR lacks quantitativity. In order to compare the elution rates, the cross sections at 10 and 25 ppm parallel to the MAS axis were obtained for the MQMAS NMR spectra before and after elution for 9 and 24 h, as shown in **Fig. 7**. The symbols *, **, and *** in the figure are considered to correspond to A, B, and C in Fig. 2, respectively, even though the glass composition is different. The degrees of residual Na for *, **, and *** were calculated to be 78, 73, and 50% for 9 h, and 0, 0, 10% for 24 h, respectively, although the signal to noise ratio was low. These results indicate that even in sodium silicate glass, the phase separation occurs microscopically, and therefore, alkali-rich domain is less durable than alkali-poor domain.

A schematic model of the elution process is shown in **Fig. 8**. There was an inhomogeneous Na^+ distribution in the sodium silicate glass; as proposed, Na_2O–$2SiO_2$ glass, A, B, and C,

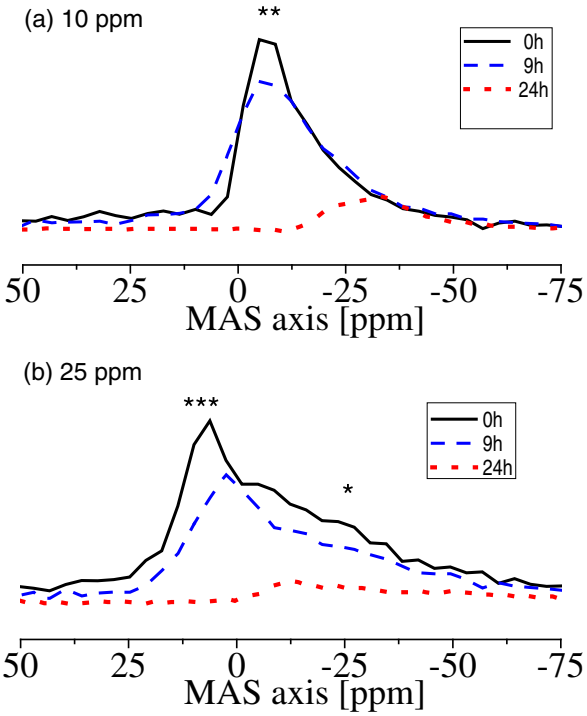

Fig. 7. (Color online) Cross sections of MQMAS spectra shown in Fig. 5 at (a) 10 ppm and (b) 25 ppm. The solid and broken lines are the cross sections shown in Figs. 5(a), 5(c) and 5(d), respectively. The symbols *, **, and *** in the figure are corresponding to A, B, and C shown in Fig. 2, respectively.

correspond to the isolated Na^+ and aggregated Na^+, which are adjacent to Q^3, and the Na^+ close to Q^2 Si, respectively. After the glass immersion in water, the Na^+ at a more aggregated site was eluted faster than that at a less aggregated site.

4.3 Mixed alkali glass

In this section, we focus on the ^{23}Na MQMAS NMR spectra of the mixed alkali glasses such as $(1-y)Na_2O$–yK_2O–$2SiO_2$ glasses. As shown in Figs. 2(a)–2(d), the fraction of Na^+ at the less aggregated site decreased with an increase in K_2O. This result can be explained in terms of the cation field strength. Because the cation field strength of Na^+ is higher than that of K^+, the energetically favorable site for Na^+ is more ionic, i.e., the aggregated site. In the case of the $(1-y)Na_2O$–yLi_2O–$2SiO_2$ glasses, the opposite tendency was observed, i.e., the fraction of Na^+ at the more aggregated site decreased with an increase in Li_2O. This result can also be explained in terms of the cation field strength.

Previously, Ingram reported a model for mixed alkali glasses based on a site memory effect and mismatch energy.[1),5),6)] During ion transport in a mixed alkali glass, an ion is transferred by hopping. The ion occupies another site where a different type of cation is present. This generates the mismatch energy. After hopping, the glass structure changes at a local level, resulting in the site memory effect. The present study clarified that there is an alkali site distribution in glass, especially in mixed alkali glass, and that a cation with a high field strength prefers to aggregate. This structural inhomogeneity generates the site mismatch energy and decreases the ion conductivity.

5. Conclusions

^{23}Na MQMAS NMR studies were conducted to investigate alkali silicate glasses. The results of the present study conducted

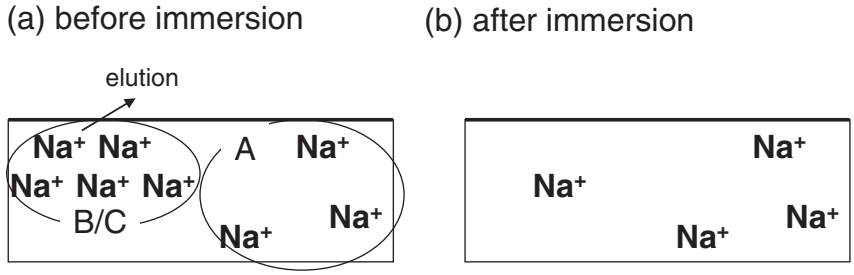

Fig. 8. Schematic model of the elution process. The elution rate of more aggregated Na^+ is higher than that of less aggregated Na^+. The aggregated Na^+ around the upper left and the isolated Na^+ around the lower right correspond to sites B/C and A shown in Fig. 2(a), respectively.

using MO calculations showed that there was an inhomogeneous distribution of Na^+ in silicate glass. This conclusion was also supported by the results of a Na^+ elution analysis, which showed that Na^+ at a more aggregated site was extracted faster than that at a less aggregated site. The results of the MQMAS experiment performed on a mixed alkali glass revealed that a cation with high field strength was likely to aggregate in mixed silicate glasses. This type of structural inhomogeneity generated site mismatch energy, which was responsible for the mixed alkali effect.

Acknowledgements This work was partially supported by the CASIO Science Promotion Foundation. The computation time was provided by the Supercomputer Laboratory, Institute for Chemical Research, Kyoto University. This work is partially supported by Grant-in-Aid for Scientific Research (C), No. 20613007, MEXT.

References

1) F. Angeli, J.-M. Delaye, T. Charpentier, J.-C. Petit, D. Ghaleb and P. Faucon, *J. Non-Cryst. Solids*, **276**, 132–137 (2000).
2) P. Maass, A. Bunde and M. D. Ingram, *Phys. Rev. Lett.*, **68**, 3064–3067 (1992).
3) F. Ali, A. V. Chadwick, G. N. Greaves, M. C. Jermy, K. L. Ngai and M. E. Smith, *Solid State NMR*, **5**, 133–143 (1995).
4) B. Gee and H. Eckert, *J. Phys. Chem.*, **100**, 3705–3712 (1996).
5) A. Bunde, M. D. Ingram and P. J. Maass, *J. Non-Cryst. Solids*, **172–174**, 1222–1236 (1994).
6) G. N. Greaves, C. R. A. Catlow, B. Vessel, J. Charnock, C. M. B. Henderson, R. Zhu, S. Qiao, Y. Wang, S. J. Gurman and S. Houde-Walter, *Int. Phys. Conf. Ser.*, **III**, 411–415 (1990).
7) S. Balasubramanian and K. J. Rao, *J. Phys. Chem.*, **97**, 8835–8838 (1993).
8) T. Uchino, T. Sakka, Y. Ogata and M. Iwasaki, *J. Non-Cryst. Solids*, **146**, 26–42 (1992).
9) T. Uchino and T. Yoko, *J. Phys. Chem. B*, **103**, 1854–1858 (1999).
10) S. Matsumoto, T. Nanba and Y. Miura, *J. Ceram. Soc. Japan*, **106**, 415–421 (1998).
11) B. Park and A. N. Cormack, *J. Non-Cryst. Solids*, **255**, 112–121 (1999).
12) E. I. Kamitsos and W. M. Risen, Jr., *J. Non-Cryst. Solids*, **65**, 333–354 (1984).
13) H. Maekawa, T. Maekawa, K. Kawamura and T. Yokokawa, *J. Non-Cryst. Solids*, **127**, 53–64 (1991).
14) J. F. Stebbins, *Solid State Ionics*, **112**, 137–141 (1998).
15) A. Bax, N. Szeverenyi and G. Maciel, *J. Magn. Reson.*, **52**, 147–152 (1983).
16) P. Florian, K. E. Vermillion, P. J. Grandinetti, I. Farnan and J. F. Stebbins, *J. Am. Chem. Soc.*, **118**, 3493–3497 (1996).
17) A. Samson, E. Lipmmaa and A. Pines, *Mol. Phys.*, **65**, 1013–1018 (1988).
18) A. Frydman and J. S. Harwood, *J. Am. Chem. Soc.*, **117**, 5367–5368 (1995).
19) S. K. Lee and J. F. Stebbins, *Geochim. Cosmochim. Acta*, **67**, 1699–1709 (2003).
20) S. K. Lee and J. F. Stebbins, *J. Phys. Chem. B*, **107**, 3141–3148 (2003).
21) Y. Tokuda, M. Takahashi and T. Yoko, Proc. 20th International Congress on Glass, Kyoto, Japan (2004).
22) A. Angelpoulou, V. Montouillout, D. Massiot and G. Kordas, *J. Non-Cryst. Solids*, **354**, 333–340 (2008).
23) T. Uchino, Y. Tokuda and T. Yoko, *Phys. Rev. B*, **58**, 5322–5328 (1998).
24) M. Kaupp, M. Bűhl and V. G. Martin, "Calculation of NMR and EPR Parameters", Wiley-VCH (2004).
25) H. Koller, G. Engelhardt, A. P. M. Kentgens and J. Sauer, *J. Phys. Chem.*, **98**, 1544–1551 (1994).
26) X. Xue and J. F. Stebbins, *Phys. Chem. Miner.*, **20**, 297–307 (1993).
27) J. P. Amoureux, C. Fernandez and S. Steuernagel, *J. Magn. Reson. A*, **123**, 116–118 (1996).
28) D. Massiot, B. Touzo, D. Trumeau, J. P. Coutures, J. Virlet, P. Florian and P. J. Grandinetti, *Solid State NMR*, **6**, 73–83 (1996).
29) Gaussian 03, Revision C.02, M. J. Frisch, G. W. Trucks, H. B. Schlegel, G. E. Scuseria, M. A. Robb, J. R. Cheeseman, J. A. Montgomery, Jr., T. Vreven, K. N. Kudin, J. C. Burant, J. M. Millam, S. S. Iyengar, J. Tomasi, V. Barone, B. Mennucci, M. Cossi, G. Scalmani, N. Rega, G. A. Petersson, H. Nakatsuji, M. Hada, M. Ehara, K. Toyota, R. Fukuda, J. Hasegawa, M. Ishida, T. Nakajima, Y. Honda, O. Kitao, H. Nakai, M. Klene, X. Li, J. E. Knox, H. P. Hratchian, J. B. Cross, V. Bakken, C. Adamo, J. Jaramillo, R. Gomperts, R. E. Stratmann, O. Yazyev, A. J. Austin, R. Cammi, C. Pomelli, J. W. Ochterski, P. Y. Ayala, K. Morokuma, G. A. Voth, P. Salvador, J. J. Dannenberg, V. G. Zakrzewski, S. Dapprich, A. D. Daniels, M. C. Strain, O. Farkas, D. K. Malick, A. D. Rabuck, K. Raghavachari, J. B. Foresman, J. V. Ortiz, Q. Cui, A. G. Baboul, S. Clifford, J. Cioslowski, B. B. Stefanov, G. Liu, A. Liashenko, P. Piskorz, I. Komaromi, R. L. Martin, D. J. Fox, T. Keith, M. A. Al-Laham, C. Y. Peng, A. Nanayakkara, M. Challacombe, P. M. W. Gill, B. Johnson, W. Chen, M. W. Wong, C. Gonzalez, and J. A. Pople, Gaussian, Inc., Wallingford CT (2004).
30) G. N. Greeves, A. Fontaine, P. Lagarde, D. Raoux and S. J. Gurman, *Nature*, **293**, 611–616 (1981).
31) W. S. McDonald and D. W. J. Cruickshank, *Acta Crystallogr.*, **22**, 37–43 (1967).
32) A. K. Pant and D. W. J. Cruickshank, *Acta Crystallogr., Sect. B: Struct. Crystallogr. Cryst. Chem.*, **24**, 13–19 (1968).
33) J. A. Tossell, *Phys. Chem. Miner.*, **27**, 70–80 (1999).
34) E. I. Kamitsos, G. D. Chryssikos, A. P. Patis and J. A. Duffy, *J. Non-Cryst. Solids*, **196**, 249–254 (1996).
35) E. I. Kamitsos, C. P. E. Varsamis and A. Vegiri, Proc. 19th International Congress on Glass, Edinburgh, United Kingdom (2001).
36) R. W. Douglas and T. M. M. El-Shamy, *J. Am. Ceram. Soc.*, **50**, 1–8 (1967).